Spatial Mapping of Velocity Power Spectra in Taylor-Couette Flow Using Ultrafast NMR Imaging

Katsumi Kose

Institute of Applied Physics, University of Tsukuba, Tsukuba-City, 305 Japan

Ultrafast NMR imaging was used to clarify spatiotemporal structures of wavy Taylor-Couette flow. NMR images designed to give a radial velocity distribution in a cross-sectional plane containing the rotation axis were successively taken at 200 ms time intervals. Distributions of velocity power-spectral components were obtained by temporal Fourier transform of the sequential velocity images. The obtained spectral maps clearly visualized the spatial structures of the wavy components in the cross-sectional plane.

PACS numbers: 47.20.−k, 47.32.−y, 47.80.+v

Flow between rotating concentric cylinders (Taylor-Couette flow) has been studied for many years to clarify the complicated but interesting character of the series of hydrodynamic transitions [1]. When rotational speed of the inner cylinder is raised gradually with the outer cylinder at rest, a transition from purely azimuthal flow (circular Couette flow) to steady toroidal vortex flow around the inner cylinder (Taylor vortex flow) is observed at a Reynolds number denoted by R_c. When the rotational speed is further increased, azimuthal traveling waves are observed on the Taylor vortices and the flow becomes time dependent above a Reynolds number denoted by R_w (wavy Taylor vortex flow). At much higher Reynolds numbers, quasiperiodic, chaotic, and turbulent flows are observed sequentially [2,3].

Although the temporal character of the time-dependent Taylor-Couette flow has been studied by laser Doppler velocimetry quite in detail [2,4], there are very few studies which have measured the spatial character of the time-dependent flow [5]. These spatial measurements, however, have been performed at most on a few lines at an instant time. Since the time-dependent flow has characteristic frequencies and characteristic spatial structures at the same time, it is highly desirable to measure the flow in a volume or in a plane at a high time resolution.

Ultrafast NMR imaging, pioneered by Mansfield and named echo-planar imaging (EPI) [6], has a remarkable advantage in flow measurements that velocity distribution in a cross-sectional plane can be measured in a very short time ($\sim$50 ms). Although this imaging technique has been applied almost solely to medical diagnosis since its invention [7], it has recently been demonstrated that EPI is a very powerful tool in studying unsteady or turbulent flow [8]. In the present paper, EPI has been used to clarify the spatiotemporal structures of the wavy Taylor-Couette flow and spatial distribution of the wavy components has been clearly visualized in a cross-sectional plane containing the rotation axis.

The inner and outer cylinders used in the experiments were high quality NMR tubes; the outer radius of the inner cylinder (r_1) was 5.00 mm and the inner radius of

the outer cylinder (r_2) was 9.00 mm. Thus the radius ratio $\eta = r_1/r_2$ was 0.556. Fluid height h of the flow cell was adjusted to 140 mm by attaching two Teflon spacers to the inner cylinder. The aspect ratio $\Gamma = h/(r_2 - r_1)$ was thus 35. The working fluid was water, longitudinal relaxation time (T_1) of the water protons being adjusted to 200 ms by dissolving some $CuSO_4$ crystals. The Reynolds number R of the flow was defined as $R = r_1 \Omega_R d/v$, where Ω_R was the rotational angular speed of the inner cylinder, $d = r_2 - r_1$, and v the kinematic viscosity of the water. In the present experiment, R_c was about 70.

When the radius ratio η is near 0.5, the transitional Reynolds number R_w is known to depend considerably on the axial wavelength λ of the Taylor vortices [9,10], which can be defined by the distance between adjacent outflow boundaries. In this experiment, various λ values (normalized by the gap width d) were observed between 1.5 and 1.8 after rapid or gradual increase of the rotational speed. Though R_w varied from $4.5R_c$ ($\lambda = 1.5$) to $6.2R_c$ ($\lambda = 1.725$), spatiotemporal behavior observed in preliminary measurements was essentially identical in this wavelength range. Thus, $\lambda = 1.65$ ($R_w \approx 5.6R_c$) was selected for the NMR measurements described below.

The flow cell was placed vertically in a superconducting NMR magnet (Oxford Instruments) with an 89 mm diameter room temperature bore operated at 4.7 T [11]. The inner cylinder was connected to an acrylic shaft which was rotated by a dc controlled motor through a pulley and belt system. Temperature of the water was kept (35 ± 0.5) °C throughout the measurements by blowing temperature controlled air over the fixed outer cylinder. NMR images were taken with a home-built NMR imaging system using the superconducting magnet and an actively shielded gradient coil (Doty Scientific). NMR images were reconstructed and observed in a real-time manner using a high-speed image reconstruction system developed in our laboratory [12].

Figure 1(a) shows the pulse sequence used in the experiments. At $t = 0$, proton spins in the cylindrical volume [Fig. 1(b), 16 mm in height] are selectively excited by the 90° pulse under the application of the magnetic field gradient along the z direction. At $t = 24$ ms, the
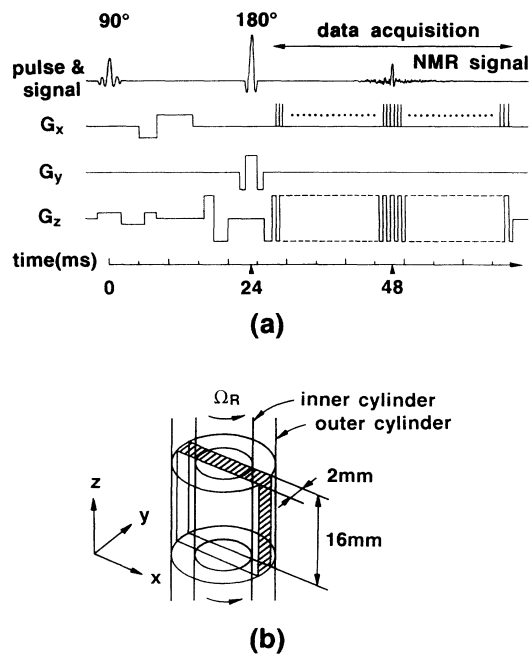
FIG. 1. (a) NMR pulse sequence used in the experiment. G_x, G_y, and G_z are magnetic field gradients along the x, y, and z directions. The data-acquisition time is 40.96 ms. (b) Cross-sectional slice imaged in the experiment.

spins in the plane containing the rotation axis (2 mm in thickness) are selectively irradiated by the 180° pulse under the application of the magnetic field gradient along the y direction. Thus, NMR signal only from the spins that *were* in the slice at $t = 24$ ms is observed at around $t = 48$ ms. This signal is used to reconstruct the distribution of nuclear magnetization in the cross section by two-dimensional Fourier transform [7].

When there is a macroscopic motion in the water, a phase shift of the nuclear magnetization *proportional* to a specified velocity component is observed [13]. This is because the precessional phase of moving spins under the oscillating magnetic field gradients is not canceled out as that of stationary spins. Although any velocity component can be measured by designing the wave form of the magnetic field gradients [8], the radial direction was selected for the following velocity measurements because the radial velocity is a major velocity component for the Taylor vortices. Thus, (almost) instantaneous radial velocity distributions were obtained from phase images calculated using the reconstructed images [14]. The velocity range detected in the experiment was from -3.0 to $+3.0$ cm/s and the velocity resolution was about 0.05 cm/s.

After the rotational speed of the inner cylinder had been raised from 0 to 132 rpm ($=5.5R_c$) and an equilibrium state with $\lambda = 1.65$ was established, 256 successive NMR images were taken at 200 and 250 ms time intervals. The measurement was repeated at $R = 5.75$, 6.0, 6.25, ... ,$8.0R_c$ after the rotational speed had been grad-
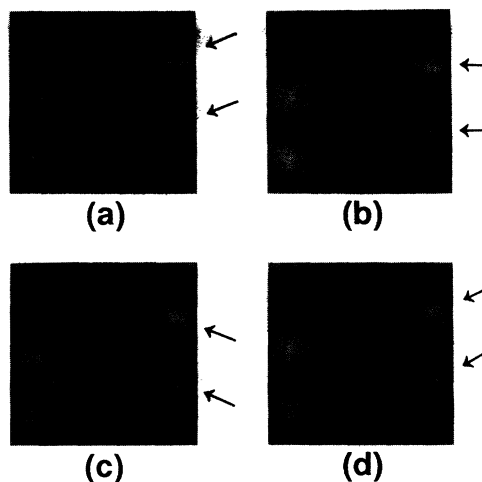

FIG. 2. Radial velocity distributions at four successive instants measured at 200 ms time intervals when $R = 6.75R_c$. The higher velocity toward the right is displayed brighter and the higher velocity toward the left is displayed darker. The velocity becomes very large at outflow boundaries of Taylor vortices. The adjacent boundaries move in phase as shown by the arrows.

ually increased to each measurement point.

Figures 2 and 3 show radial velocity distributions at four successive instants measured at 200 ms time intervals when $R = 6.75R_c$. The center of the images is located 40 mm apart from the lower edge of the cell and the field of view of the images is 19.2 mm×19.2 mm. The number of the image matrix is 64×64; thus the pixel size is 0.3 mm×0.3 mm. Each side of the gap thus contains about 13 pixels along the radial direction. In these im-
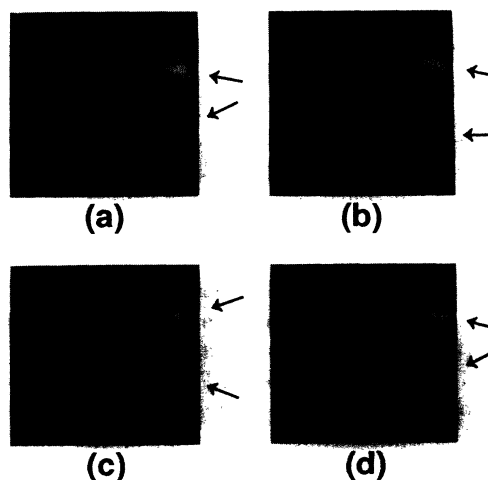

FIG. 3. Radial velocity distributions at four successive instants measured under the same condition as that of Fig. 2. The adjacent boundaries, however, move in antiphase as shown by the arrows.

ages, the higher velocity toward the right is displayed brighter and the higher velocity toward the left is displayed darker. Although a large geometric distortion due to magnetic field inhomogeneity is observed near the upper left corner of the images, high speed flows from the inner to the outer cylinder are clearly visualized. These "jets" correspond to outflow boundaries of Taylor vortices [9,10]. The maximum speed in the jets is about 2.5 cm/s in these images.

As shown by the arrows in the figures, the adjacent outflow boundaries move in phase in Fig. 2 and antiphase in Fig. 3. These two modes are calculated and named "harmonic jet" and "subharmonic jet" by Jones [10]. Both modes were observed at Reynolds numbers from $5.75R_c$ to $8.0R_c$: In most cases the in-phase modes were observed first and spontaneous transitions to the antiphase mode were observed at fixed Reynolds numbers. The transition of the reverse direction, however, was not observed in these experiments. Since the motional phases of the wavy jet motion in the right and left gaps were always opposite to each other as shown in the figures, the azimuthal wave number m is odd. Although the value of m cannot be determined by this experiment, m is considered to be 1 from the earlier studies [9,10].

We can obtain spatial distributions of velocity power-spectral components by temporal Fourier transform of the sequential velocity images. Figures 4 and 5 show total velocity power spectra integrated over the cross section and four typical power-spectral maps selected from 128 spectral maps. These results are calculated from se-

quences of 256 images measured at 200 ms time intervals. As shown in Fig. 4, wavy frequency components are seen at $\omega \approx 0.6\Omega_R$ ($=\omega_1$) and its second harmonics are seen at aliased frequencies. This aliasing has been confirmed by spectral maps obtained from image sequences measured at 250 ms time intervals.

Spatial distributions of these wavy spectral components are shown in Figs. 5(c) and 5(d). These maps have been obtained for the subharmonic mode. Spatial distribution of the ω_1 component for one outflow boundary consists of two lobes symmetrically separated by the horizontal radial line going from the origin of the jet. We denote this line by L_j. This pattern can be understood by considering the up-and-down oscillation of the outflow boundaries as shown in Figs. 2 and 3. This distribution agrees with that of the eigenfunction of the velocity perturbation calculated under the condition, $\eta = 0.56$, $\lambda = 1.6$, and $R = 5.35R_c$ [16], which is close to the present experimental condition. Spatial distribution of the $2\omega_1$ component for one outflow boundary consists of three lobes. This spatial pattern may be understood to consist of two $2\omega_1$ oscillations, the center lines of which are located slightly apart from the line L_j.

Although similar spatial maps as Fig. 5 were obtained also at the Reynolds numbers up to $8.0R_c$, measurements at much higher Reynolds numbers where quasiperiodic or chaotic flows will be observed were difficult in the present system. This is mainly because of the experimental limitation that the data acquisition time (40.96 ms) is relatively long comparing with the fluid speed in the cross
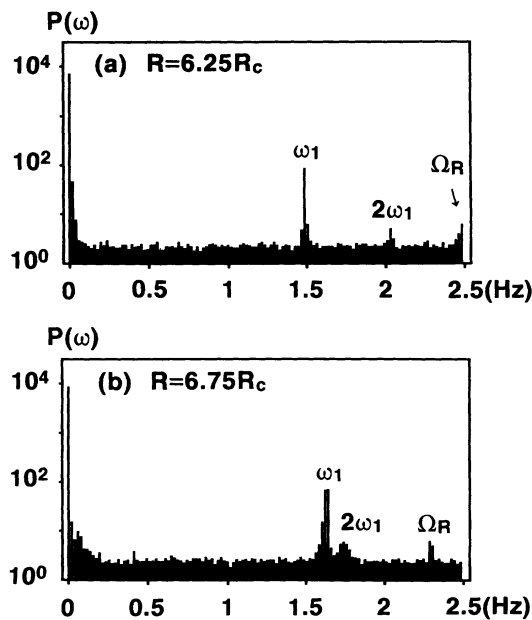

FIG. 4. Velocity power spectra integrated over the cross section. Slightly broadened spectra at ω_1 and $2\omega_1$ in (b) are due to the result that two wavy modes are contained in the image sequence as shown in Figs. 2 and 3.

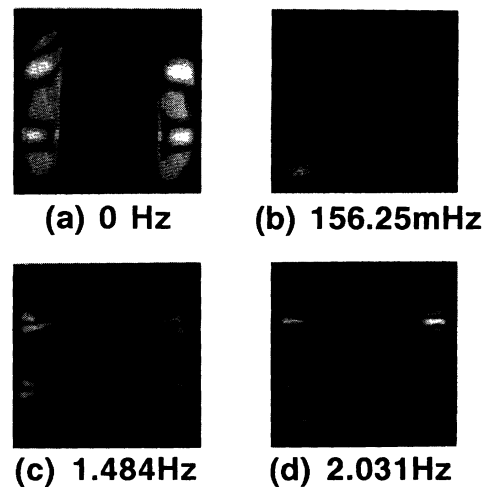

(a) 0 Hz   (b) 156.25mHz

(c) 1.484Hz   (d) 2.031Hz

FIG. 5. Typical spatial distributions of velocity power-spectral components obtained at $R = 6.25R_c$. Time averaged velocity distribution (a) shows high-speed flows at the outflow boundaries. When there is no specific spectral component, the spectral map shows a random noisy distribution except near the inner cylinder and the lower left corner [(b)] [15]. Though the $2\omega_1$ component is seen at the aliased frequency (2.031 Hz), the true frequency is 2.969 Hz.

section at such high Reynolds numbers. If the measurement system is scaled up, a major part of the experimental difficulties could be cleared.

In conclusion, dynamical spatial structures of the wavy Taylor-Couette flow have been clearly visualized using ultrafast NMR imaging. Experiments at much higher Reynolds numbers using this technique are promising future extensions of this work.

[1] R. C. DiPrima and H. L. Swinney, in *Hydrodynamic Instabilities and the Transition to Turbulence*, edited by H. L. Swinney and J. P. Gollub (Springer, Berlin, 1981).

[2] A. Brandstater and H. L. Swinney, Phys. Rev. A 35, 2207 (1987).

[3] D. P. Lathrop, J. Fineberg, and H. L. Swinney, Phys. Rev. A 46, 6390 (1992).

[4] J. P. Gollub and H. L. Swinney, Phys. Rev. Lett. 35, 927 (1975); P. R. Fensternmacher, H. L. Swinney, and J. P. Gollub, J. Fluid Mech. 94, 103 (1979).

[5] R. W. Walden and R. J. Donnelly, Phys. Rev. Lett. 42, 301 (1979); G. Ahlers, D. S. Cannel, and M. A. Dominguez Lerma, Phys. Rev. Lett. 49, 368 (1982); Y. Takeda, W. E. Fischer, K. Kobashi, and T. Takada, Exp. Fluids 13, 199 (1992).

[6] P. Mansfield, J. Phys. C 10, L55 (1977).

[7] R. Rzedzian and I. L. Pykett, Am. J. Roentgenol. 149, 245 (1987); M. K. Stehling, R. Turner, and P. Mansfield, Science 254, 43 (1991).

[8] K. Kose, J. Phys. D 23, 981 (1990); Phys. Rev. A 44,

[9] A. Lorenzen, G. Pfister, and T. Mullin, Phys. Fluids 26, 10 (1983); A. Lorenzen and T. Mullin, Phys. Rev. A 31, 3463 (1985).

[10] C. A. Jones, J. Fluid Mech. 157, 135 (1985).

[11] In the present experimental configuration, since the Chandrasekhar number which characterizes the magnetohydrodynamic effect is of the order of 10^{-2}, the effect of magnetic field on the flow is negligible: P. Tabeling, J. Fluid Mech. 112, 329 (1981).

[12] K. Kose and T. Inouye, Meas. Sci. Technol. 3, 1161 (1992).

[13] J. R. Singer, J. Phys. E 11, 281 (1978); A. Caprihan and E. Fukushima, Phys. Rep. 198, 195 (1990). In general, the observed phase shift is proportional to a linear combination of time derivatives of the position, such as velocity, acceleration, jerk, etc. For usual experimental conditions, however, the higher terms can be neglected within experimental errors.

[14] Since maximum radial velocity observed in this study is about 3 cm/s, the proton spins travel across about 4 pixels during the data-acquisition time. However, image blur or measurement error caused by this motion is small because major spatial Fourier components concentrate on a short period around $t = 48$ ms.

[15] High intensities in these regions are due to apparent velocity fluctuation produced by a calculation threshold under which the phase value is set to zero. In these regions, reconstructed pixel intensities fluctuate around the threshold in the image sequences.
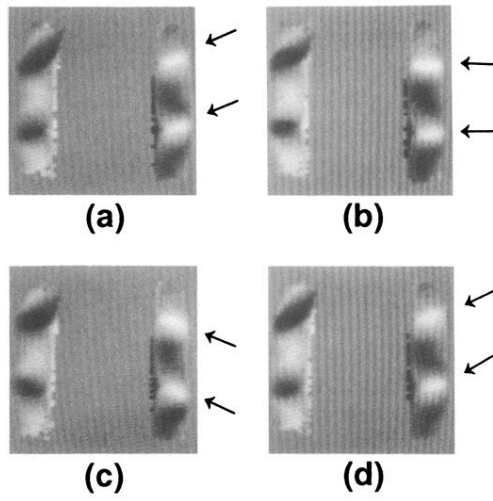
[16] Figure 8 in Ref. [10].

2495 (1991); J. Magn. Reson. 92, 631 (1991); 96, 596 (1992); 98, 599 (1992).

FIG. 2. Radial velocity distributions at four successive instants measured at 200 ms time intervals when $R = 6.75 R_c$. The higher velocity toward the right is displayed brighter and the higher velocity toward the left is displayed darker. The velocity becomes very large at outflow boundaries of Taylor vortices. The adjacent boundaries move in phase as shown by the arrows.
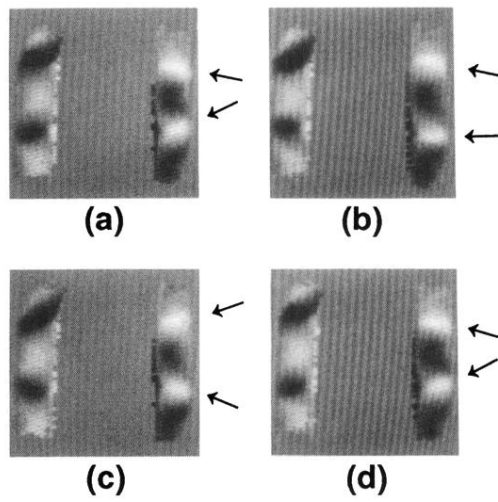
FIG. 3. Radial velocity distributions at four successive instants measured under the same condition as that of Fig. 2. The adjacent boundaries, however, move in antiphase as shown by the arrows.
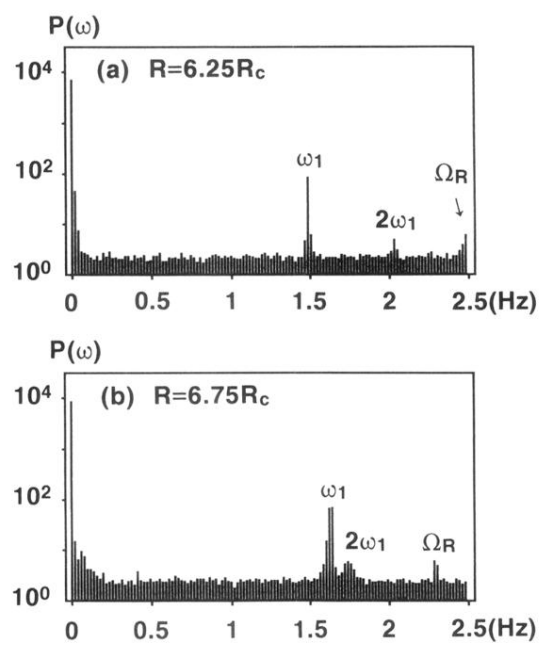
FIG. 4. Velocity power spectra integrated over the cross section. Slightly broadened spectra at ω_1 and $2\omega_1$ in (b) are due to the result that two wavy modes are contained in the image sequence as shown in Figs. 2 and 3.

(a) 0 Hz   **(b) 156.25mHz**
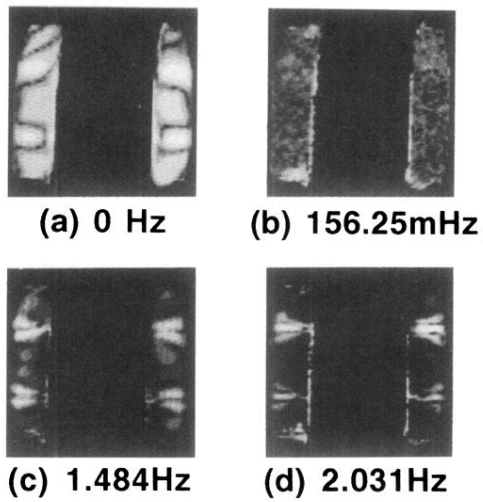
(c) 1.484Hz   **(d) 2.031Hz**

FIG. 5. Typical spatial distributions of velocity power-spectral components obtained at $R = 6.25 R_c$. Time averaged velocity distribution (a) shows high-speed flows at the outflow boundaries. When there is no specific spectral component, the spectral map shows a random noisy distribution except near the inner cylinder and the lower left corner [(b)] [15]. Though the $2\omega_1$ component is seen at the aliased frequency (2.031 Hz), the true frequency is 2.969 Hz.